Supplementary material for "Unconventional level attraction in cavity axion polariton of antiferromagnetic topological insulator"

Yang Xiao[1,*], Huaiqiang Wang[2,3,*], Dinghui Wang[2], Ruifeng Lu[4], Xiaohong Yan[5], Hong Guo[6], C. -M. Hu[7], Ke Xia[8], Haijun Zhang[2,3,†] and Dingyu Xing[2,3]

[1]*College of Science, Nanjing University of Aeronautics and Astronautics, Nanjing 210016, China*
[2]*National Laboratory of Solid State Microstructures and Physics School, Nanjing University, Nanjing 210093, China*
[3]*Collaborative Innovation Center of Advanced Microstructures, Nanjing University, Nanjing 210093, China*
[4]*Department of Applied Physics, Nanjing University of Science and Technology, Nanjing 210094, China*
[5]*School of Material Science and Engineering, Jiangsu University, Zhenjiang, 212013, China*
[6]*Department of Physics, McGill University, Montreal, Quebec H3A 2T8, Canada*
[7]*Department of Physics and Astronomy, University of Manitoba, Winnipeg R3T 2N2, Canada and*
[8]*Beijing Computational Science Research Center, Beijing 100193, China*[*]

In this supplementary material, we will present more details of numerical and analytical methods of transmission calculation. Figures explaining the results but not shown in main texts are also given in this material.

NUMERICAL METHOD

This part is for theoretical and numerical details of calculating the transmission spectrum S_{21} of electromagnetic wave inside the cavity. The calculation consists of three steps. First, we need to know the propagating state in AFM. Due to the axion-photon coupling, the propagating state is no longer pure photon state, but an axion polariton. So, we calculate the wave vector of propagation state based on the modified equations of dynamical axion and the Maxwell's equations. Second, with the propagating state, we build the transfer matrix connecting the amplitude of electromagnetic field at input port with that at output port. In the third step, we solve for the propagation of electromagnetic wave inside the AFM-embedded cavity using scattering matrix method. The axion mode can be a long-wavelength mode discussed in main texts or a short-wavelength mode discussed in this supplementary material.

Lagrangian and dynamical equations

The total Lagrangian density of the axion-photon coupled system can be written as

$$\begin{aligned}\mathcal{L}_{\text{tot}} =&\mathcal{L}_{\text{Maxwell}} + \mathcal{L}_{\text{topo}} + \mathcal{L}_{\text{axion}} \\ =&\frac{1}{8\pi}\left(\epsilon\mathbf{E}^2 - \frac{1}{\mu}\mathbf{B}^2\right) + \frac{\alpha}{4\pi^2}\left(\theta_0 + \delta\theta\right)\mathbf{E}\cdot\mathbf{B} + g^2 J\left[(\partial_t\delta\theta)^2 - (v_i\partial_i\delta\theta)^2 - m^2\delta\theta^2\right],\end{aligned} \tag{1}$$

where $\mathbf{E}$ and $\mathbf{B}$ are electric and magnetic fields, respectively, ϵ and μ represent dielectric constant and magnetic permeability, $\alpha = e^2/\hbar c_0$ is the fine-structure constant, c_0 is the speed of light in the vacuum, θ_0 denotes the static part of the axion field, and $\delta\theta$ represents the massive dynamical axion field originating from the longitudinal spin-wave mode with material-dependent stiffness J, velocity v_i, mass m, and coefficient g. Through the Euler-Lagrangian equation, we can obtain

$$\nabla \cdot \mathbf{D} = 4\pi\rho - \frac{\alpha}{\pi}(\nabla\delta\theta \cdot \mathbf{B}) \tag{2}$$

$$\nabla \times \mathbf{H} = \frac{1}{c_0}\frac{\partial \mathbf{D}}{\partial t} + \frac{4\pi}{c_0}\mathbf{j} + \frac{\alpha}{\pi}\left((\nabla\delta\theta \times \mathbf{E}) + \frac{1}{c_0}(\partial_t\delta\theta)\,\mathbf{B}\right) \tag{3}$$

$$\nabla \times \mathbf{E} = -\frac{1}{c_0}\frac{\partial \mathbf{B}}{\partial t} \tag{4}$$

$$\nabla \cdot \mathbf{B} = 0 \tag{5}$$

$$\frac{\alpha}{8\pi^2 g^2 J}\mathbf{E} \cdot \mathbf{B} = \frac{\partial^2}{\partial t^2}\delta\theta - v^2\nabla^2\delta\theta + m^2\delta\theta, \tag{6}$$

where

$$\begin{gathered}\mathbf{D} = \mathbf{E} + 4\pi\mathbf{P} = \epsilon\mathbf{E} \\ \mathbf{H} = \mathbf{B} - 4\pi\mathbf{M} = \frac{1}{\mu}\mathbf{B}.\end{gathered} \tag{7}$$

Equations (2)-(5) correspond to the modified Maxwell equation, and Eq. (6) describes the equation of motion for $\delta\theta$.

When an external magnetic field is applied, by inserting Eq. (7) into Eq. (3) and adding ∂_t to both sides of Eq. (3), we get

$$\partial_t(\nabla \times \frac{\mathbf{B}}{\mu}) = \frac{1}{c_0}\frac{\partial^2 \epsilon\mathbf{E}}{\partial t^2} + \frac{\alpha}{\pi}\partial_t\left((\nabla\delta\theta \times \mathbf{E}) + \frac{1}{c_0}(\partial_t\delta\theta)\,\mathbf{B}\right), \tag{8}$$

where $\mathbf{j} = 0$ is assumed. With the help of Eq. (4), and the relation

$$\nabla \times (\nabla \times \mathbf{a}) = \nabla(\nabla \cdot \mathbf{a}) - \nabla^2\mathbf{a} \tag{9}$$

we obtain

$$\frac{\partial^2}{\partial t^2}e - c^2\nabla^2 e + \frac{\alpha B}{\pi\epsilon}\frac{\partial^2}{\partial t^2}\delta\theta = 0, \tag{10}$$

where terms coupling $\mathbf{E}$ and $\mathbf{B}$ to $\delta\theta$ are kept to linear order, e is the electric component parallel to $\mathbf{B}$, and $c = c_0/(\sqrt{\epsilon\mu})$.

By including the damping of axion mode, we can rewrite Eq. (6)

$$\frac{\partial^2}{\partial t^2}\delta\theta - v^2\nabla^2\delta\theta + m^2\delta\theta + \Gamma\frac{\partial\delta\theta}{\partial t} - \frac{\alpha B}{8\pi^2 g^2 J}e = 0. \tag{11}$$

Propagating states

In the long wavelength limit, the wave vector is small. The long-wavelength axion mode represents uniform distribution of axion field within the material. Since $\nabla^2\delta\theta = -k^2\delta\theta \approx 0$, we can neglect the dispersion of axion mode. By solving Eq. (10) and Eq. (11) simultaneously, we derive one propagating state, i.e.

$$c^2k^2 = \omega^2\frac{\omega^2 + i\Gamma\omega - (b^2 + m^2)}{\omega^2 + i\Gamma\omega - m^2}, \tag{12}$$

with $b^2 = \alpha^2 B^2/(8\pi^3\epsilon g^2 J)$.

Transfer matrix

With Eq. (4), we have $ke = -\omega\mu h$. So, we can define the impedance of electromagnetic wave

$$Z = \frac{e}{h} = -\frac{\omega\mu}{k}. \tag{13}$$

In the material, there exist the left-going and right-going propagating states. So, the field can be expressed by linear combination of these two states, i.e.

$$h = (h^+ e^{-ikx} + h^- e^{ikx}), \tag{14}$$

$$e = Z(h^+ e^{-ikx} - h^- e^{ikx}). \tag{15}$$

Next, we consider the boundary condition of electromagnetic wave at the left (x=0) and right (x=d) surfaces,

$$\begin{cases} h^0 = h^+ + h^- \\ e^0 = Z(h^+ - h^-) \\ h^d = h^+ e^{-ikd} + h^- e^{ikd} \\ e^d = Z(h^+ e^{-ikd} - h^- e^{ikd}) \end{cases} \tag{16}$$

By eliminating h^+ and h^-, one can obtain

$$\begin{pmatrix} e^d \\ h^d \end{pmatrix} = M_s \begin{pmatrix} e^0 \\ h^0 \end{pmatrix} = \begin{pmatrix} cos(kd) & -iZsin(kd) \\ -\frac{i}{Z} sin(kd) & cos(kd) \end{pmatrix} \begin{pmatrix} e^0 \\ h^0 \end{pmatrix}, \tag{17}$$

where M_s is the transfer matrix in the material.

Since the AFM-embedded cavity contains the left air region, the material region and the right air region, we have three transfer matrices. From input port to output port of cavity, the total transfer matrix is written as

$$M = M_0 M_s M_0 = \begin{pmatrix} A & B \\ C & D \end{pmatrix}, \tag{18}$$

where M_0 is the transfer matrix of the air region.

Transmission coefficient

The transfer matrix describes the relation between the fields at two ports. In order to obtain transmission coefficient S_{21}, we have to know the in-coming and out-going wave at input port (port A) and output port (port B) of cavity,

$$\begin{pmatrix} e_A^- \\ e_B^- \end{pmatrix} = \begin{pmatrix} S_{AA} & S_{AB} \\ S_{BA} & S_{BB} \end{pmatrix} \begin{pmatrix} e_A^+ \\ e_B^+ \end{pmatrix}, \tag{19}$$

where $-(+)$ represents the direction from the cavity (outside) to outside(cavity).

The scattering matrix is

$$\begin{pmatrix} S_{AA} & S_{AB} \\ S_{BA} & S_{BB} \end{pmatrix} = \begin{pmatrix} \frac{A+B/Z_0-CZ_0-D}{A+B/Z_0+CZ_0+D} & \frac{2(AD-BC)}{A+B/Z_0+CZ_0+D} \\ \frac{2}{A+B/Z_0+CZ_0+D} & \frac{-A+B/Z_0-CZ_0+D}{A+B/Z_0+CZ_0+D} \end{pmatrix}. \tag{20}$$

In order to create standing wave (cavity resonance) inside the cavity, the electromagnetic wave should experience strong reflection at each port. In this work, the reflectivity of intracavity photon is described by R and we set $R_A = R_B = R \approx 1$.

The transmission coefficient is defined as the amplitude ratio of outgoing wave at port B and incident wave at port A, i.e.

$$S_{21} = \frac{e_{Bx}^-}{e_{Ax}^{inc}} = (1 - R^2) \frac{S_{BA}}{(1 - R_A S_{AA})(1 - R_B S_{BB}) - R_A R_B S_{AB} S_{BA}}. \tag{21}$$

Fig. S1 shows the $|S_{21}|$ spectrum obtained with the numeric method given in the above section. One can see two odd modes (510 and 570 GHz) and one even mode (540 GHz). The most obvious characteristics is the anticrossing gap of LR for even mode. But for odd mode, the interaction is small. The enlarged plots in the right side show LA and a larger gap for R=0.99 than for R=0.999.

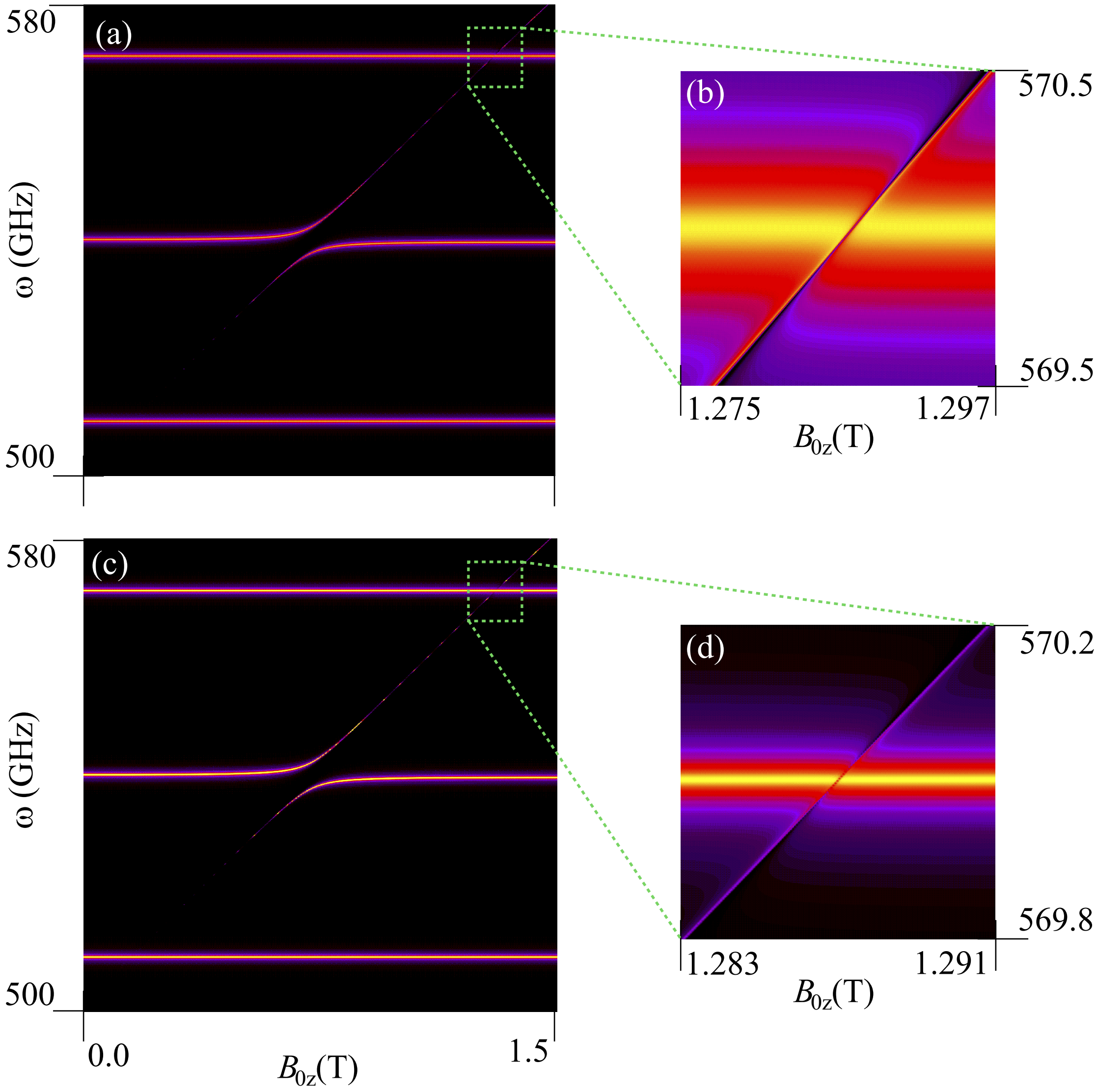

FIG. S1: (Color online) $|S_{21}|$ spectra of 0.1μm-thick AFM calculated from the numeric method. The enlarged view of box region in left panels are given in the right. Top and bottom panels are for R=0.99 and R=0.999.

ANALYTICAL METHOD

In this part, we derive the analytic expressions of S_{21} based on the Taylor expansion. We rewrite Eq. (20) as

$$\begin{pmatrix} S_{AA} & S_{AB} \\ S_{BA} & S_{BB} \end{pmatrix} = e^{2jk_0 l} \begin{pmatrix} \frac{-sin(k_s l_s)(Z_0^2 - Z_s^2)}{(Z_0^2+Z_s^2)sin(k_s l_s)+2jZ_0 Z_s cos(k_s l_s)} & \frac{2jZ_0 Z_s}{(Z_0^2+Z_s^2)sin(k_s l_s)+2jZ_0 Z_s cos(k_s l_s)} \\ \frac{2jZ_0 Z_s}{(Z_0^2+Z_s^2)sin(k_s l_s)+2jZ_0 Z_s cos(k_s l_s)} & \frac{-sin(k_s l_s)(Z_0^2 - Z_s^2)}{(Z_0^2+Z_s^2)sin(k_s l_s)+2jZ_0 Z_s cos(k_s l_s)} \end{pmatrix}, \tag{22}$$

where $k_0 = \frac{\omega}{c}$, $k_s = \frac{\omega}{c}\sqrt{\epsilon_s \mu_s}$, $Z_0 = \frac{\omega \mu_0}{k_0} = c\mu_0$ and $Z_s = \frac{c\mu_0}{\sqrt{\epsilon_s \mu_s}}$.

Substituting the elements of Eq. (22) into Eq. (21), we obtain

$$S_{21} = \frac{F}{G}, \tag{23}$$

where

$$F = 2je^{-2jk_0 l}(Z_0 Z_s)^{-1}((Z_0^2 + Z_s^2)sin(k_s l_s) + 2jZ_0 Z_s cos(k_s l_s)) \tag{24}$$

and

$$G = f_0 + f_R. \tag{25}$$

The part f_0 corresponds to those terms assuming $R = 1$ while f_R gives the remaining terms which are related to (1-R). The detailed forms are

$$\begin{aligned}
f_0 &= 4 - 4cos^2(k_s l_s)e^{-4jk_0 l} \\
&+ 4j\frac{Z_0}{Z_s}sin(k_s l_s)cos(k_s l_s)(1 + e^{-2jk_0 l})e^{-2jk_0 l} \\
&+ -4j\frac{Z_s}{Z_0}sin(k_s l_s)cos(k_s l_s)(1 - e^{-2jk_0 l})e^{-2jk_0 l} \\
&+ \left[\frac{Z_0}{Z_s}(e^{-2jk_0 l} + 1)sin(k_s l_s) + \frac{Z_s}{Z_0}(e^{-2jk_0 l} - 1)sin(k_s l_s)\right]^2
\end{aligned}$$

and

$$\begin{aligned}
f_R &= -2(1 - R)e^{-2jk_0 l}\left[\frac{Z_0}{Z_s} - \frac{Z_s}{Z_0}\right]\left[\frac{Z_0}{Z_s} + \frac{Z_s}{Z_0}\right]sin^2(k_s l_s) \\
&- 4j(1 - R)e^{-2jk_0 l}\left[\frac{Z_0}{Z_s} - \frac{Z_s}{Z_0}\right]sin(k_s l_s)cos(k_s l_s) \\
&- (1 - R^2)\left[\frac{Z_0}{Z_s} - \frac{Z_s}{Z_0}\right]^2 sin^2(k_s l_s) \\
&- 4(1 - R^2).
\end{aligned}$$

The analytic expression of S_{21} is obtained by performing the Taylor expansion. First, we expand the function $sin(k_s l_s)$ and $cos(k_s l_s)$

$$\begin{aligned}
sink_s l_s &\approx k_s l_s - \frac{1}{6}k_s^3 l_s^3 + \cdots = \sum_n \frac{(-1)^n}{(2n+1)!}(k_s l_s)^{2n+1}, \\
cosk_s l_s &\approx 1 - \frac{1}{2}k_s^2 l_s^2 + \cdots = \sum_n \frac{(-1)^n}{(2n)!}(k_s l_s)^{2n}.
\end{aligned} \tag{26}$$

Second, we expand the function $e^{-2jk_0 l}$ at cavity resonance frequency $\omega_{CR} = \frac{cq\pi}{2l+l_s}$

$$\begin{aligned}
e^{-2jk_0 l} &= e^{-j\frac{2l}{c}\omega} = e^{j\frac{l_s}{c}\omega}e^{-j\frac{2l+l_s}{c}\omega} \\
&\approx e^{j\frac{l_s}{c}\omega}\left[e^{-j\frac{2l+l_s}{c}\omega_{CR}} + (-j\frac{2l+l_s}{c})e^{-j\frac{2l+l_s}{c}\omega_{CR}}(\omega - \omega_{CR}) + \cdots\right] \\
&= e^{-j\frac{2l+l_s}{c}\omega_{CR}}e^{j\frac{l_s}{c}\omega}\left[1 + (-j\frac{2l+l_s}{c})(\omega - \omega_{CR}) + \cdots\right] \\
&= e^{-jq\pi}\sum_n \frac{(j\frac{l_s}{c}\omega)^n}{n!}\sum_m \frac{(\Delta\omega_C)^m}{m!}
\end{aligned} \tag{27}$$

where $\Delta\omega_C = (-j\frac{2l+l_s}{c})(\omega - \omega_{CR})$. q is odd (even) for odd (even) mode.

Odd mode

Leading terms in the expression of denominator are given below according to l_s^n. High-order terms are depicted in Fig. 2c and 2f of main texts. For odd mode, we have

(i) n=0

$$-8\Delta\omega_C - 8\Delta\omega_C^2 + \cdots . \tag{28}$$

(ii) n=1

$$\begin{aligned}
&4j(\frac{l_s}{c}\omega)(\epsilon\mu-1)\Delta\omega_C,\\
&+6j(\frac{l_s}{c}\omega)(\epsilon\mu-1)\Delta\omega_C^2,\\
&+\frac{14}{3}j(\frac{l_s}{c}\omega)(\epsilon\mu-1)\Delta\omega_C^3,\\
&+\frac{5}{2}j(\frac{l_s}{c}\omega)(\epsilon\mu-1)\Delta\omega_C^4,
\end{aligned}\tag{29}$$

(iii) n=2

$$\begin{aligned}
&(\frac{l_s}{c}\omega)^2(\epsilon\mu-1)^2\Delta\omega_C^2,\\
&+(\frac{l_s}{c}\omega)^2(\epsilon\mu-1)^2\Delta\omega_C^3,\\
&+\frac{7}{12}(\frac{l_s}{c}\omega)^2(\epsilon\mu-1)^2\Delta\omega_C^4,
\end{aligned}\tag{30}$$

(iv) n=3

$$\begin{aligned}
&\frac{2}{3}j(\frac{l_s}{c}\omega)^3(\epsilon\mu-1),\\
&-\frac{2}{3}j(\frac{l_s}{c}\omega)^3(\epsilon\mu-1)(\epsilon\mu-2)\Delta\omega_C,\\
&-j(\frac{l_s}{c}\omega)^3(\epsilon\mu-1)(\epsilon\mu-\frac{4}{3})\Delta\omega_C^2,\\
&-\frac{1}{9}j(\frac{l_s}{c}\omega)^3(\epsilon\mu-1)(7\epsilon\mu-8)\Delta\omega_C^3,\\
&-\frac{1}{36}j(\frac{l_s}{c}\omega)^3(\epsilon\mu-1)(15\epsilon\mu-16)\Delta\omega_C^4,
\end{aligned}\tag{31}$$

(v) n=4

$$\begin{aligned}
&\frac{1}{3}(\frac{l_s}{c}\omega)^4(\epsilon\mu-1)^2,\\
&+(\frac{l_s}{c}\omega)^4(\epsilon\mu-1)^2\Delta\omega_C,\\
&-\frac{1}{6}(\frac{l_s}{c}\omega)^4(\epsilon\mu-1)^2(2\epsilon\mu-7)\Delta\omega_C^2,\\
&-\frac{1}{6}(\frac{l_s}{c}\omega)^4(\epsilon\mu-1)^2(2\epsilon\mu-5)\Delta\omega_C^3,\\
&-\frac{1}{72}(\frac{l_s}{c}\omega)^4(\epsilon\mu-1)^2(14\epsilon\mu-31)\Delta\omega_C^4,
\end{aligned}\tag{32}$$

(vi) f_R

$$\begin{aligned}
f_R &= 4j(\frac{l_s}{c}\omega)(\epsilon\mu-1)(1-R)\\
&+(\frac{l_s}{c}\omega)^2(\epsilon\mu-1)^2(1-R)^2\\
&+2(\frac{l_s}{c}\omega)^2(\epsilon\mu-1)^2(1-R)\Delta\omega_C.
\end{aligned}\tag{33}$$

With the 1^{st}, 2^{nd} and f_R terms, we can obtain an approximate expression

$$S_{21}=\frac{\omega-m'}{(\omega-\omega_c')(\omega-\omega_1')},\tag{34}$$

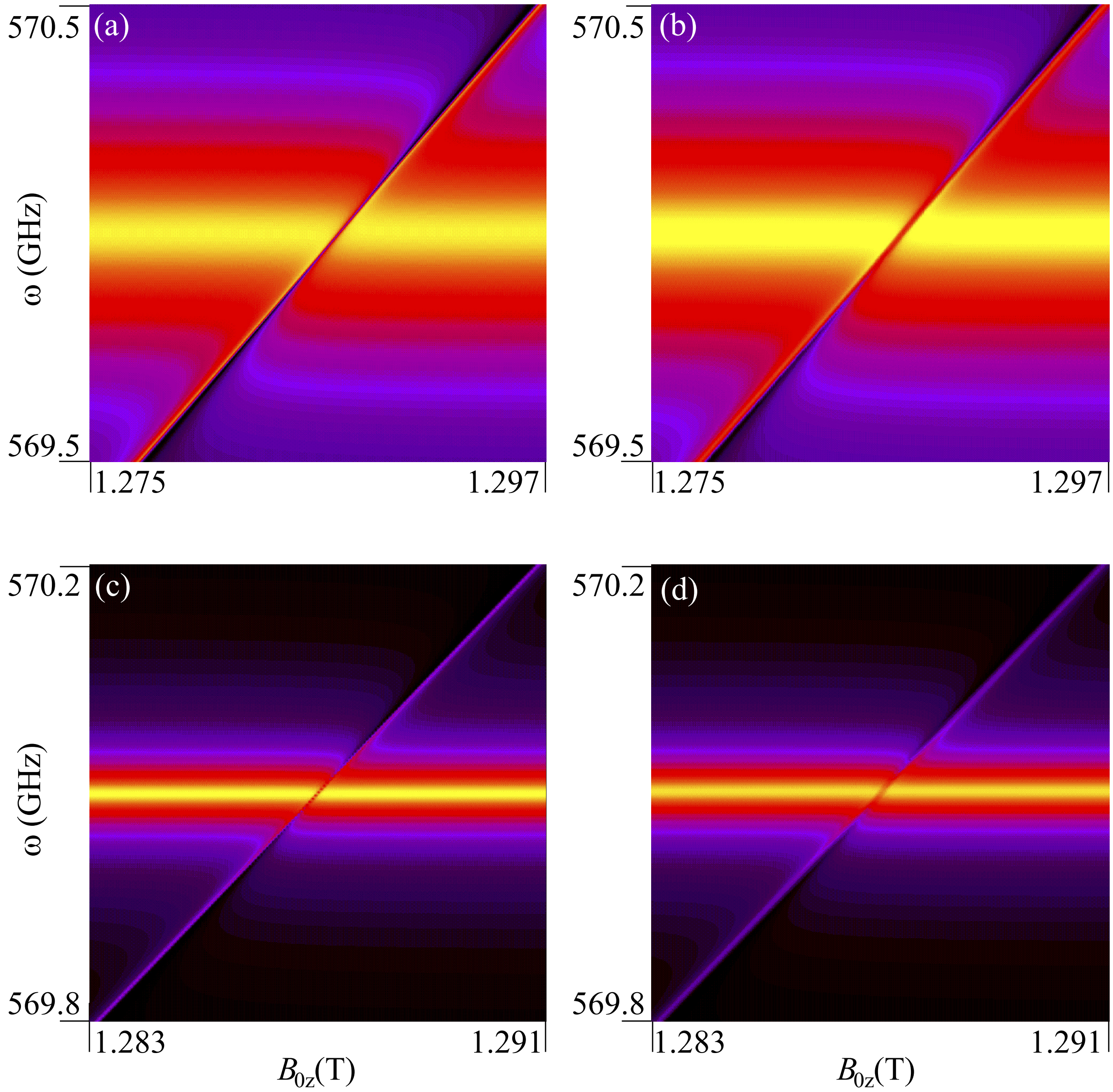

FIG. S2: $|S_{21}|$ spectra of 0.1μm-thick AFM of odd mode calculated with (left) numeric method and (right) the formula $S_{21} = \frac{\omega - m'}{(\omega-\omega_c')(\omega-\omega_1')}$. Top and bottom panels are for R=0.99 and R=0.999.

which is exactly Eq. (5) with renormalized line-width in main texts. Here, $\omega_c' = \omega_c - i\eta(1-R)$, $\omega_1' = \omega_1 - i\zeta(1-R)$ and $m' = m - i\Gamma\omega$. Two parameters are $\eta = 4/A$ and $\zeta = 4D/[A(A+D)]$ with $A = 8l/c$ and $D = 2l^2 l_s \epsilon b^2/c^3$. Eq. (34) describes the numeric results very well as shown in Fig. S2.

Fig. S3 shows that, as R increases, the $|S_{21}|$ spectrum evolves from LA (R=0.99 and 0.999) into LR (R=0.9999). The physical mechanism of LA is originated from the nonlinear type-II interaction (the first- and second-order) and the dissipation. But as R approaches unity, the mechanism from dissipation vanishes. Therefore, the third-order term of type-I nonlinear interaction starts to contribute and produces LR.

Even mode

For even mode, we have

(i) n=0

$$-8\Delta\omega_C + \cdots . \tag{35}$$

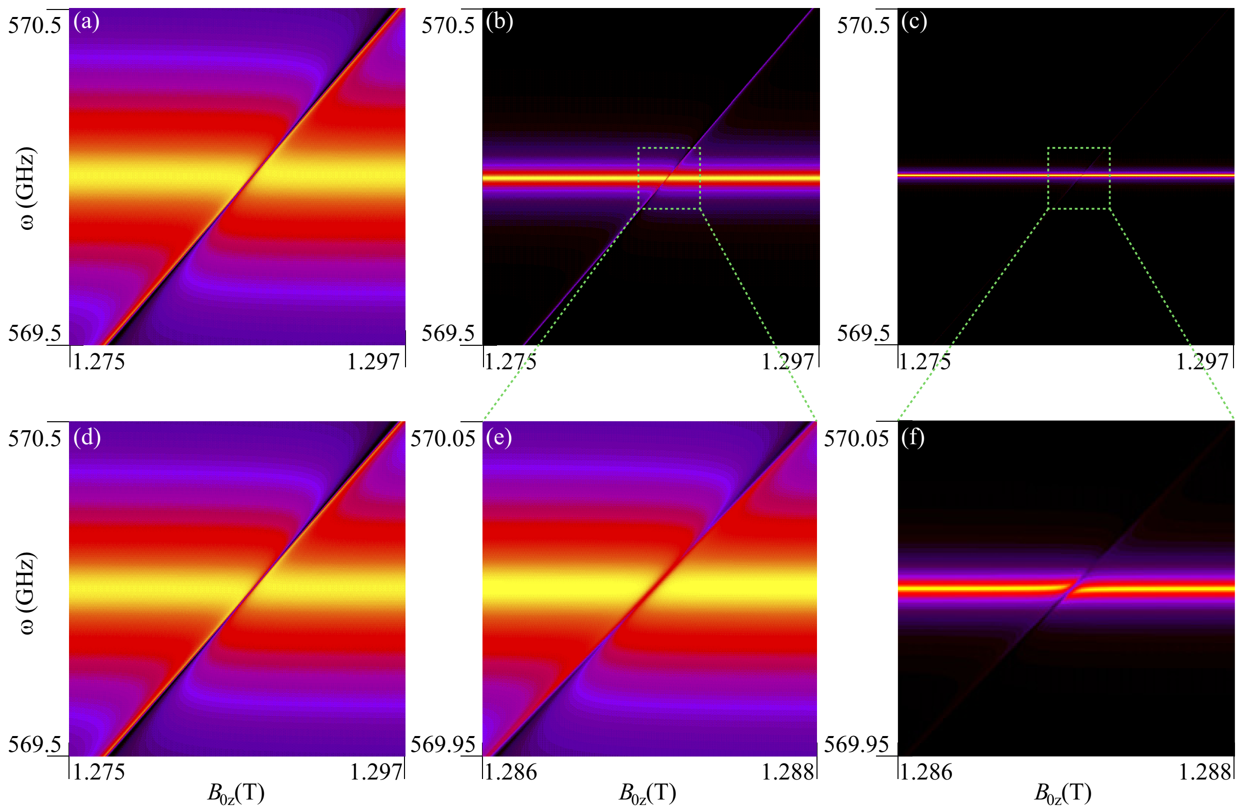

FIG. S3: $|S_{21}|$ spectra of $0.1\mu m$-thick AFM of odd mode calculated with numeric method for R=0.99 (left), R=0.999 (middle) and R=0.9999 (right). Bottom panels are the enlarged views of box region in top panels. Note that (a) and (d) are the same figures.

(ii) n=1

$$\begin{aligned} &8j(\frac{l_s}{c}\omega)(\epsilon\mu-1) \\ &+12j(\frac{l_s}{c}\omega)(\epsilon\mu-1)\Delta\omega_C, \end{aligned} \tag{36}$$

(iii) n=2

$$\begin{aligned} &4(\frac{l_s}{c}\omega)^2(\epsilon\mu-1)^2 \\ &+4(\frac{l_s}{c}\omega)^2(\epsilon\mu-1)^2\Delta\omega_C, \end{aligned} \tag{37}$$

(ii) n=3

$$\begin{aligned} &-\frac{4}{3}j(\frac{l_s}{c}\omega)^3(\epsilon\mu-1)(\epsilon\mu-\frac{1}{2}), \\ &-2j(\frac{l_s}{c}\omega)^3(\epsilon\mu-1)(\epsilon\mu-\frac{2}{3})\Delta\omega_C, \end{aligned} \tag{38}$$

(iii) n=4

$$\begin{aligned} &-\frac{1}{3}(\frac{l_s}{c}\omega)^4(\epsilon\mu-1)(\frac{4}{3}\epsilon\mu+1)(\epsilon\mu+1), \\ &-(\frac{l_s}{c}\omega)^4(\epsilon\mu-1)(\frac{4}{3}\epsilon\mu-\frac{5}{3})(\epsilon\mu-1)\Delta\omega_C, \end{aligned} \tag{39}$$

The denominator of even mode is dominated by the linear term and can be written as

$$G=-8\Delta\omega_C+8j(\frac{l_s}{c}\omega)(\epsilon\mu-1)=16j\frac{l}{c}\left[(\omega-\omega_C)-\frac{g^2}{\omega-m}\right], \tag{40}$$

from which one can obtain the coupling strength of LR with $g^2 = \frac{\epsilon b^2 l_s}{4l}$.

SHORT-WAVELENGTH MODE

Propagating mode

When the wavelength is finite, i.e. k is large, we should consider the dispersion of axion mode explicitly. For convenience, we define $f = \frac{v}{c}$. Solving Eq. (10) and Eq. (11) simultaneously gives rise to two propagating state, i.e.

$$c^2k_\pm^2 = \frac{[f^2\omega^2 + (\omega^2 + i\gamma\omega - m^2)] \pm \sqrt{[f^2\omega^2 - (\omega^2 + i\gamma\omega - m^2)]^2 + 4b^2\omega^2 f^2}}{2f^2}. \tag{41}$$

Transfer matrix

In the presence of two propagating modes, the electric and magnetic field are written as

$$h = \sum_{n=1}^{2}(h_n^+ e^{-ik_n x} + h_n^- e^{ik_n x}),$$
$$e = \sum_{n=1}^{2} Z_n(h_n^+ e^{-ik_n x} - h_n^- e^{ik_n x}).$$

The field at the left (x=0) and right (x=d) surfaces of AFM are

$$\begin{cases} h^0 = \sum_{n=1}^{2}(h_n^+ + h_n^-) \\ e^0 = \sum_{n=1}^{2} Z_n(h_n^+ - h_n^-) \\ h^d = \sum_{n=1}^{2}(h_n^+ e^{-ik_n d} + h_n^- e^{ik_n d}) \\ e^d = \sum_{n=1}^{2} Z_n(h_n^+ e^{-ik_n d} - h_n^- e^{ik_n d}) \end{cases} \tag{42}$$

Obviously, it is insufficient to derive the transfer matrix based on the above four equations. Therefore, two extra equations should be supplied. This is accomplished by introducing the boundary condition of axion field at surfaces of AFM.

The simplest boundary condition of axion field is

$$\delta\theta = 0, \quad x = 0, \tag{43}$$
$$\delta\theta = 0, \quad x = d, \tag{44}$$

indicating that the axion fields at two surfaces are totally pinned.

With Eq. (10), the relation between e and $\delta\theta$ is given by

$$\delta\theta = Pe = \frac{\epsilon\pi(c^2k^2 - \omega^2)}{\alpha B\omega^2} e. \tag{45}$$

The boundary conditions shown in Eq. (43) and (44) give rise to two extra equations

$$\begin{cases} \delta\theta^0 = \sum_{n=1}^{2} P_n(h_n^+ - h_n^-) = 0 \\ \delta\theta^d = \sum_{n=1}^{2} P_n(h_n^+ e^{-ik_n d} - h_n^- e^{ik_n d}) = 0. \end{cases} \tag{46}$$

To obtain the transfer matrix, we rewrite Eq. (46) and the third and the fourth equations of Eq. (42) to construct a matrix equation

$$(J)\begin{pmatrix} h_1^+ \\ h_1^- \\ h_2^+ \\ h_2^- \end{pmatrix} = \begin{pmatrix} h^d \\ e^d \\ 0 \\ 0 \end{pmatrix}, \tag{47}$$

where J is expressed by

$$J = \begin{pmatrix} e^{-ik_1 d} & e^{ik_1 d} & e^{-ik_2 d} & e^{ik_2 d} \\ Z_1 e^{-ik_1 d} & -Z_1 e^{ik_1 d} & Z_2 e^{-ik_2 d} & -Z_2 e^{ik_2 d} \\ Z_1 P_1 & -Z_1 P_1 & Z_2 P_2 & -Z_2 P_2 \\ Z_1 P_1 e^{-ik_1 d} & -Z_1 P_1 e^{ik_1 d} & Z_2 P_2 e^{-ik_2 d} & -Z_2 P_2 e^{ik_2 d} \end{pmatrix}. \tag{48}$$

With Eq. (47), we can substitute $h^{\pm}_{n=1,2}$ expressed by h^d and e^d into the first and the second equations of Eq. (42). The transfer equation is therefore given by

$$M_s = \begin{pmatrix} A & B \\ C & D \end{pmatrix}^{-1}, \tag{49}$$

where

$$\begin{aligned} A &= Z_1 J^{-1}_{12} - Z_1 J^{-1}_{22} + Z_2 J^{-1}_{32} - Z_2 J^{-1}_{42}, \\ B &= Z_1 J^{-1}_{11} - Z_1 J^{-1}_{21} + Z_2 J^{-1}_{31} - Z_2 J^{-1}_{41}, \\ C &= J^{-1}_{12} + J^{-1}_{22} + J^{-1}_{32} + J^{-1}_{42}, \\ D &= J^{-1}_{11} + J^{-1}_{21} + J^{-1}_{31} + J^{-1}_{41}. \end{aligned}$$

With the transfer matrix, S_{21} is calculated using the same method as those given in Sec. ID.

Fig. S4 shows the $|S_{21}|$ spectra of standing wave axion mode with negative and positive slopes of an 1 μm-thick AFM film. Since the axion field is pinned at top and bottow surfaces, the field profile follows a sinusoidal function and thus only the odd-order standing wave mode can survive. Further, we notice that the gap size is almost constant with the order n for negative-slope axion modes but attenuates rapidly for positive-slope one. The reasons are two-fold. First, as the order n increases, the part of axion field participating in the axion-photon interaction decreases with the function of $\propto \frac{1}{n}$. Second, the resonance field B_0 increases with n for negative-slope axion modes and thereby promote the coupling strength b. These two factors are depicted in Fig. S4c and results in the unusual behavior of axion-photon coupling. This result is important for thin film-based devices since the nonuniform distribution is usually unavoidable for realistic axion material.

* Electronic address: zhanghj@nju.edu.cn

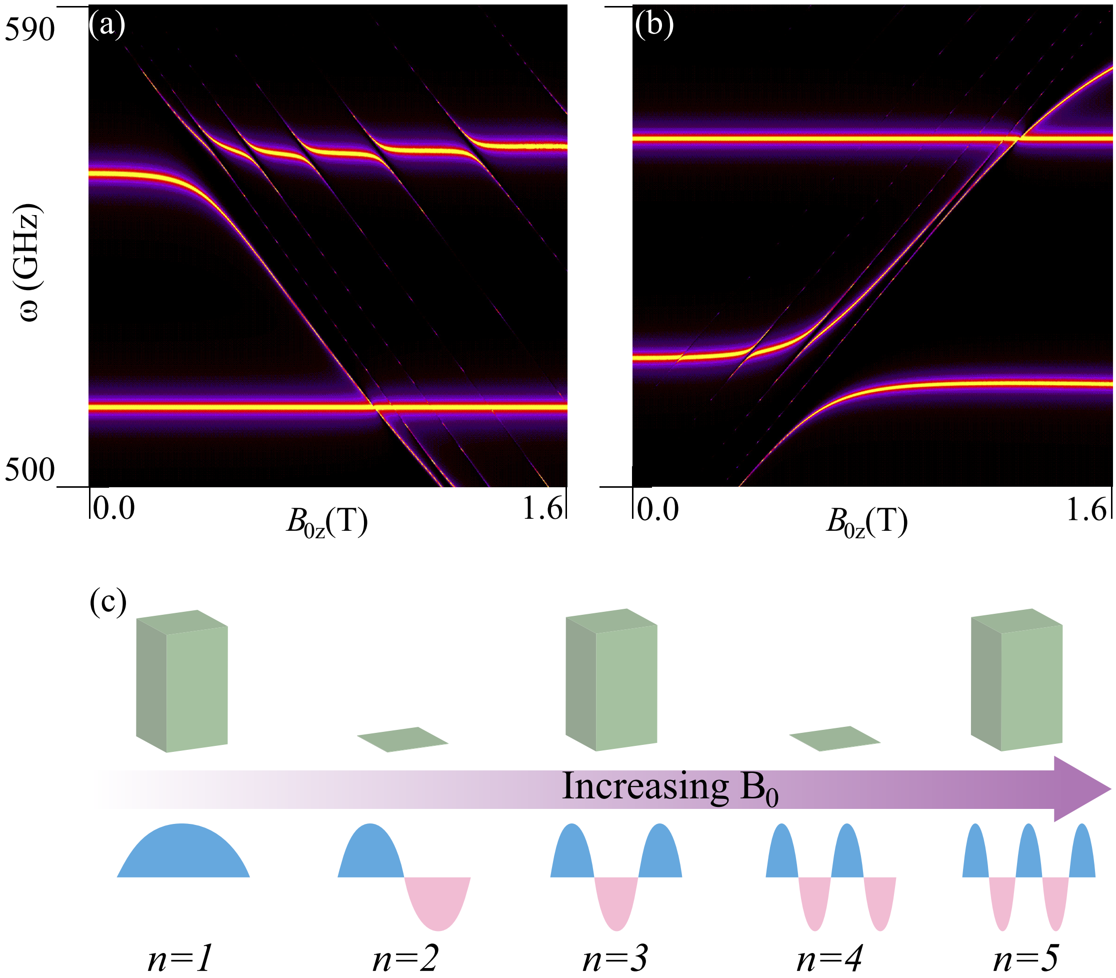

FIG. S4: $|S_{21}|$ spectra of $1\mu m$-thick AFM for standing wave axion mode with (a) negative and (b) positive slopes. (c) Two factors determine the unusual behavior in (a). The first is the increase in resonance magnetic field for negative-slope axion mode. The second is that the effective part of dynamic axion field coupling to electromagnetic field scales as $\frac{1}{n}$. n is the order of standing wave mode.